Eng. Sci., 2020, 11, 76-84

Engineered Science

DOI: https://dx.doi.org/10.30919/es8d0023

Melanin Sensitized Nanostructured ZnO Photoanodes for Efficient Photoelectrochemical Splitting of Water: Synthesis and Characterization

Priti Vairale,[1] Vidhika Sharma,[1] Bharat Bade,[1] Ashish Waghmare,[1] Pratibha Shinde,[1] Ashvini Punde,[1] Vidya Doiphode,[1] Rahul Aher,[1] Subhash Pandharkar,[1] Shruthi Nair,[1] Vijaya Jadkar,[1] Pandit Shelke,[2] Mohit Prasad[3] and Sandesh Jadkar[3,*]

Abstract

Herein, we report the synthesis of different ZnO nanostructures using chemical bath deposition method by changing the molar concentration of zinc precursor. The synthesized films were characterized using X-ray diffraction, UV-Visible spectroscopy, and scanning electron microscopy for different physico-chemical characterization. The obtained ZnO nanostructures were sensitized with melanin. We found that melanin incorporation in ZnO nanostructures extended the absorbance spectra into visible region. The maximum photocurrent density was recorded with ZnO film deposited for the molar concentration of 0.2 M. The rise might be attributed to the increased specific surface area, crystallinity, charge transfer and reduced recombination losses. The effects of synthetic melanin dye on all the synthesized samples had also been studied for the photoelectrochemical (PEC) study. Melanin incorporated ZnO photo-anodes showed a photocurrent density about twice that of bare ZnO photo-anode under one sun illumination. The obtained results demonstrated that melanin incorporated ZnO can be considered as a potential material for photo-anodes for photosplitting of water.

Keywords: Chemical bath deposition; ZnO; Melanin; Photoelectrochemical cell; Nanostructures.
Received: 25 May 2020; Accepted: 24 June 2020.
Article type: Research article.

1. Introduction

Due to the pressing need for alternative and clean energy generation systems, solar-hydrogen production through photoelectrochemical (PEC) splitting of water is a highly pursued research area. PEC cells require incorporation of improved photo-catalysts onto light-absorbing semiconductors to realize photo-anodes for efficient solar to chemical energy conversion process. To have efficient water splitting, one needs to find a robust and efficient photo-anode which can enhance the overall PEC process. In 1972, *Fujishima and Honda*[1] initiated the research activity in PEC systems. Since then a large number of metal-semiconductor oxide materials such as TiO_2,[2] Fe_2O_3,[3] $BiVO_4$,[4] WO_3,[5] Cu_2O[6] and ZnO[7] have been investigated for realizing efficient photo-anodes for water splitting. Among all the metal oxide semiconductors, zinc oxide (ZnO) has evolved as the most attractive material for PEC water splitting application.[8-12] ZnO is a non-toxic n-type semiconductor with a direct bandgap (3.2 eV), has well-aligned band edges, large piezoelectric constants, high electron mobility (~ 2 x10^3 cm^2/Vs at 50 K), high exciton binding energy (~ 60 meV), high thermal conductivity, and is reasonably stable.[13] The material has been also employed successfully in various applications such as in heat-protecting windows, front contact of liquid crystal displays, field-effect transistors, UV-sensitive and solar-blind photo-detectors, gas sensors, and in energy conversion devices.[14] As per the solar hydrogen production, one of the major drawbacks of ZnO is its poor absorption in the visible region. To enhance absorption different types of ZnO nanostructures such as nano-particles, nano-tubes, nano-flowers, nano-wires, nano-rods, nano-disks, nano-plates,

[1] *School of Energy Studies, Savitribai Phule Pune University, Pune 411007, India*
[2] *Department of Physics, Baburaoji Gholap College, New Saghavi, Pune 411027, India*
[3] *Department of Physics, Savitribai Phule Pune University, Pune 411007, India*
* *E-mail: sandesh@physics.unipune.ac.in (S. Jadkar)*

nano-spheres, nano-sheets, nano-spikes, etc. have been synthesized by different methods such as molecular beam epitaxy,[15] spray pyrolysis[16] pulsed laser deposition,[17] hydrothermal,[18] chemical bath deposition,[19] electrodeposition,[20] etc. Among these, chemical bath deposition has the advantage of being operational at low temperature, low cost, suitable for large area deposition for industrial applications, and environmentally benign.

Melanin is a conjugated biomacromolecule[21] and a universal biopolymeric pigment exhibiting interesting physicochemical properties[22] such as strong absorption in UV-Visible region,[23] semiconducting properties,[24] redox activity,[25] metal-ion chelation activity,[26] hydrophilicity activity,[27] hydration dependent conductivity,[28] free radical properties,[29] etc. It has been reported that synthetic melanins can be produced with physical and chemical properties very similar to those of natural melanin.[30,31] As a result, it has been used in UV filters,[32] solid-state organic electrochemical transistors,[33] metal-insulator devices,[34] flexible supercapacitors,[35] pH sensors,[36] engineered electrodes,[37] moisture sensors,[38] E-ink for display devices,[39] and edible batteries,[40] etc. Due to strong absorption in UV-Visible region and semiconductor behaviour, melanin has received considerable attention in recent years for the development of opto-electronic devices. However, to date, there are few reports on the development of melanin-based devices for artificial photosynthesis, utilizing its unique optical and electrical properties. Recently, the development of melanin-based organic/inorganic hybrid photoanodes for solar water oxidation was reported by *Lee et al.*[41] with remarkably improved photocurrent density. Furthermore, previous studies on the controlled morphology and dye sensitization have shown improved photo-response of ZnO in the visible region. To the best of our knowledge, till date, no one has taken into account the synergistic effect of controlled morphology of ZnO and melanin dye. With this motivation, melanin sensitized ZnO nanostructured films have been synthesized for PEC splitting of water. In this paper, we report the synthesis of different nanostructures of ZnO using chemical bath deposition method by changing the molar concentration of zinc precursor. The influence of synthetic melanin on all the synthesized ZnO nanostructures has been studied for PEC activity. We found that melanin incorporation in ZnO nanostructures extends the absorbance spectra into the visible region, thus their use in PEC splitting of water in visible light is possible. Melanin incorporated ZnO photo-anodes showed photocurrent density about ~ 2 times higher than that of the bare ZnO photo-anode under one sun illumination. The obtained results demonstrate that melanin incorporated ZnO can be considered as a potential material for photoanodes for photosplitting of water.

2. Experimental

2.1 Preparation of ZnO thin films

For the chemical bath deposition of ZnO thin films, a solution was prepared by dissolving different molar concentration (0.2, 0.15, 0.1 and 0.08 M) of zinc nitrate [$Zn(NO_3)_2 \cdot 6H_2O$], in 100 mL of distilled water and 3ml of 7.4 M triethanolamine was added in the precursor solution, which was stirred for 15 min, then few drops (25 %) of ammonia was added to obtain pH ~ 11. The solution was again stirred at 80°C for 3 h and a transparent solution was obtained. Florine doped thin oxide (SnO_2:F, FTO) glass slides (Resistivity ~ 10 Ω-cm, dimensions: 4 cm×3 cm) were used as substrate for thin film deposition. The substrates were cleaned by the ultrasonication process for 10 min using the following solvents in the given order: acetone, ethanol and double-distilled water. The substrates were dried by dry nitrogen (N_2) gas. The above cleaning procedure gives good adhesion of the film on the substrate.

2.2 Preparation of melanin thin films

In the present study, thin films of melanin were prepared via potentiostatic method using three-electrode electrochemical cells (Metrohm Autolab: PGSTAT302N). Films were deposited on a 1 cm x 1 cm x 2 mm fluorine-doped tin oxide (FTO) substrate which acts as a working electrode. Graphite was used as a counter electrode. The distance between the working electrode and the counter electrode was kept 1 cm. Saturated calomel was used as a reference electrode. The potential time and deposition time were kept constant at 2 V and 3 h, respectively. For the synthesis of melanin thin films, we have used synthetic melanin powder M8631-250 mg (Sigma-Aldrich) directly without further purification. The melanin powder was dissolved in dimethyl sulfoxide and methanol solution ($DMSO/CH_3OH$ = 1:20) at 0.2 mg/mL concentration. The FTO substrates were initially cleaned with double distilled water and finally cleaned with acetone, ethanol and double distilled water (DDW) by keeping in ultrasonic bath for 10 min each. The above cleaning procedure gives good adhesion of the film to the substrate. The pH of the solution was kept at 6.8. After synthesis, samples were rinsed extensively with double distilled water and then dried in ambient air.

2.3 Film characterization

The crystalline structure of the samples was studied through glancing angle X-ray diffractometer (Bruker AXS D8 Advance, Germany; angular accuracy 0.001°, angular resolution > 0.01°) equipped with graphite monochromator, a mirror at a fixed incidence angle of 1-5° and CuK_α (λ = 1.5406 Å) as the radiation source. Scanning electron micrographs (SEM) of samples were recorded using JEOL JSMS 6360 scanning electron microscope. Absorption spectra of films were recorded with respect to the bare substrate by employing double beam UV-Visible spectrophotometer (JASCO V-670) in the range 300-800 nm. Raman spectra were recorded with Raman spectroscopy instrument (Horiba Jobin-Yvon's LabRAM-HR) in the range 300-800 cm^{-1}. Potentiostat (Metrohm Autolab PGSTAT302N) and 300 W Xenon arc lamp (PEC L01), light source was employed to record current-voltage (I-V) characteristics of the cell, both under darkness and illumination. The EIS and Mott-Schottky measurements were carried out using

same potentiostat (Model: FRA 32M). The saturated calomel electrode (SCE) reference values were converted to the reversible hydrogen electrode (RHE) reference electrode values using the following equation,

$$E_{RHE} = E_{SCE} + 0.243 + 0.059 \text{ x pH} \quad (1)$$

where E_{SCE} is the applied potential vs. SCE and E_{SCE} is the standard electrode potential of SCE (0.243 V at 25 °C). The thickness of ZnO and Melanin films were measured by using a non-contact profilometer (KLA-Tencor, P-16+). The thickness of ZnO film was found in the range of 300-500 nm whereas the thickness of Melanin film was ~ 325 nm.

3 Results and discussion

3.1 Scanning electron microscopy (SEM) analysis

To visualize the surface morphology of ZnO thin films scanning electron microscopy (SEM) was used. The SEM images of ZnO thin films at different molar concentrations of zinc nitrate are shown in Fig. 1. As seen from Fig. 1, all films are uniform and have compact grain structures, without crack or holes and covers the entire substrate surface. A significant change can be clearly seen in the growth morphology of the film when the zinc nitrate concentration is increased. The film deposited at a zinc acetate concentration of 0.08 M [Fig. 1(a)] shows the growth of mesoporous ZnO. When the concentration of zinc nitrate is increased to 0.1 M, well-aligned hexagonal shaped ZnO nano-rods evolve as shown in Fig. 1(b). When the concentration of zinc nitrate increased further to 0.15 M or 0.20 M flower or sheet type ZnO nanostructures are obtained [See Fig. 1(c) and Fig. 1(d)]. Formation of flower or sheet type ZnO nanostructures indicates non-uniform nucleation on the substrate surface and faster growth kinetics from the individual nucleation centers, which is due to a higher electrolyte concentration. We think that unlike the case of nano-flower or nano-sheet type ZnO structure, a lower concentration of zinc nitrate used for the growth of nano-rods or mesoporous ZnO produces more uniform nucleation and growth.

Fig. 1(e) illustrates the SEM micrograph of melanin thin film grown by the electrochemical method. As seen from the Fig. 1(e), the surface morphology of melanin shows aggregation of melanin macro-molecules. Furthermore, the melanin film exhibits a dense and conformal layer without surface defects such as voids or cracks.

3.2 X-ray diffraction (XRD) analysis

X-ray diffraction (XRD) and Raman spectroscopy are used to confirm the formation and to analyze the structural properties of ZnO and melanin thin films prepared by chemical bath deposition method. Typical XRD pattern recorded for all the synthesized ZnO thin films at different concentrations of zinc nitrate is shown in Fig. 2(a). As seen from XRD pattern major diffraction peaks appear at 2θ ~ 32.01°, 33.93°, 36.43°, 47.76°, 61.78°, 66.79°, 68.19°, and 69.2° corresponding to (100), (002), (101), (102), (103), (200), (112), and (201), respectively, of hexagonal wurtzite ZnO (JCPDS data card # 36-1451), suggesting its dominant evolution. The films deposited at 0.15 M and 0.2 M, i.e. for ZnO nano-flowers and ZnO nano-sheets, (002) and (100) peaks appear to be more intense, indicating their preferred growth directions. The relative intensity of (002) peak is found to increase for the ZnO films deposited at zinc nitrate concentration of 0.10 M (ZnO nano-rods) and 0.08 M (Mesoporous ZnO) particularly with respect to the reference pattern, suggesting the beginning of the c-axis oriented growth. For ZnO nano-flowers, the relative intensity of the (002) peak is found to be the singular most intense feature, with the (100) and (101) peak intensities drastically reduced, which is as expected from their better-aligned c-axis growth. The average crystallite size ($d_{X\text{-ray}}$) was calculated using *Debye-Scherer* equation,[42]

$$d_{x\text{-}ray} = \frac{0.9\,\lambda}{\beta \cos\theta_B} \quad (2)$$

where λ is the wavelength of Cu-K_α line and β is the full width at half maximum (FWHM) of diffraction peak. The average crystallite size shows a decreasing trend with an increase in zinc nitrate molar concentration and the values were found in the range of 20.4 to 18.1 nm.

Fig. 2(b) shows XRD pattern of synthetic melanin thin film deposited using chemical bath deposition method. The pattern shows a broad shoulder centered at 2θ ~ 21.4°. This diffraction peak is characteristic diffraction peak of natural melanin or synthetic melanin.[43]

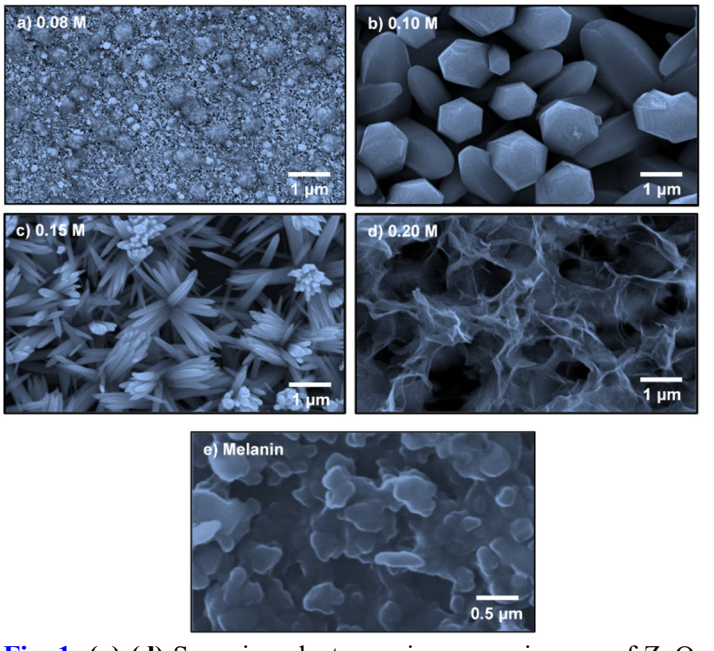

Fig. 1 **(a)-(d)** Scanning electron microscopy images of ZnO nanostructures for different molar concentrations of zinc nitrate and **(e)** Scanning electron microscopy images of melanin prepared using electrodeposition method.

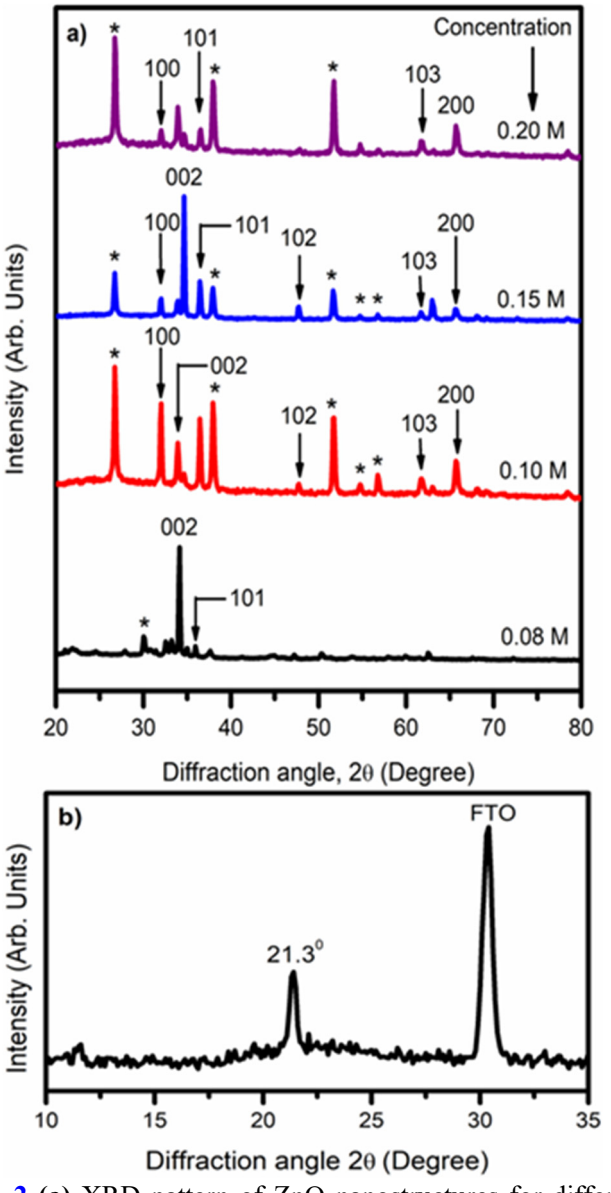

Fig. 2 **(a)** XRD pattern of ZnO nanostructures for different molar concentrations of zinc nitrate and **(b)** XRD pattern of synthetic melanin. (*) indicate the XRD diffraction peaks of SnO_2:F on which ZnO layer is deposited.

3.3 Raman spectroscopy analysis

Raman scattering is generally sensitive to the structural properties including atomic vacancy and defects and also to the size and shapes of the nanoscale materials. The structure of any material predominantly depends on the nature of the preparation methods and their corresponding parameters. Fig. 3(a) shows the Raman spectra for ZnO thin films deposited at different molar concentrations of zinc nitrate. As seen from the Fig. 3(a), the spectra show Raman lines centered at ~ 438 cm^{-1} and ~573 cm^{-1} for all ZnO films. These lines are assigned to ZnO E_2 (high) and A_1 longitudinal optical (LO) mode respectively,[44] which confirms the formation of wurtzite ZnO structure. The Raman mode ~ 573 cm^{-1} can be attributed to the residual stress, structural disorder and crystal defect in the ZnO films. The weak broad (E_{2L}-E_{2H}) feature at 331 cm^{-1} is observed only in the case of nano-sheets (and not in other synthesized nanostructures of ZnO) likely because of their weaker E_{2L} and E_{2H} modes. The existence of Raman mode at ~ 631 cm^{-1} is debatable. However, it has been reported that such local modes are possible for frequency above 600 cm^{-1} i.e. above optical mode.[45]

Fig. 3(b) shows the Raman spectrum of melanin thin films prepared by the electrochemical process in the range of 1000-1800 cm^{-1}. It consists of two bands, centred at ~ 1600 cm^{-1} (G-band) and ~ 1350 cm^{-1} (D-band). For quantitative analysis, Raman data has been deconvoluted using *Levenberg-Marquardt* algorithm[46,47] with Gaussian/Lorentzian sum functions. As seen from the de-convoluted spectra, the peaks ~ 1726 cm^{-1}, ~ 1606 cm^{-1} and ~ 1513 cm^{-1} can be assigned to the stretching vibration of the C=O band of ketone groups attached to the quinine, the aromatic C=C stretching modes of the basic indole structure and the C=N stretching and/or the N-H bending modes, respectively.[48] The C-N stretching band of indole was centered at 1340 cm^{-1}. The band at 1407 cm^{-1} correspond to the O-H deformation or a combination of bands caused by the C-O stretching and O-H deformation of the carboxylic acid.[49,50] The C-OH phenolic stretching and C-O stretching of the carboxylic are observed at 1204 cm^{-1}. These results are in good agreement with the previously reported data which confirms the formation of melanin thin films using the electrochemical deposition method.

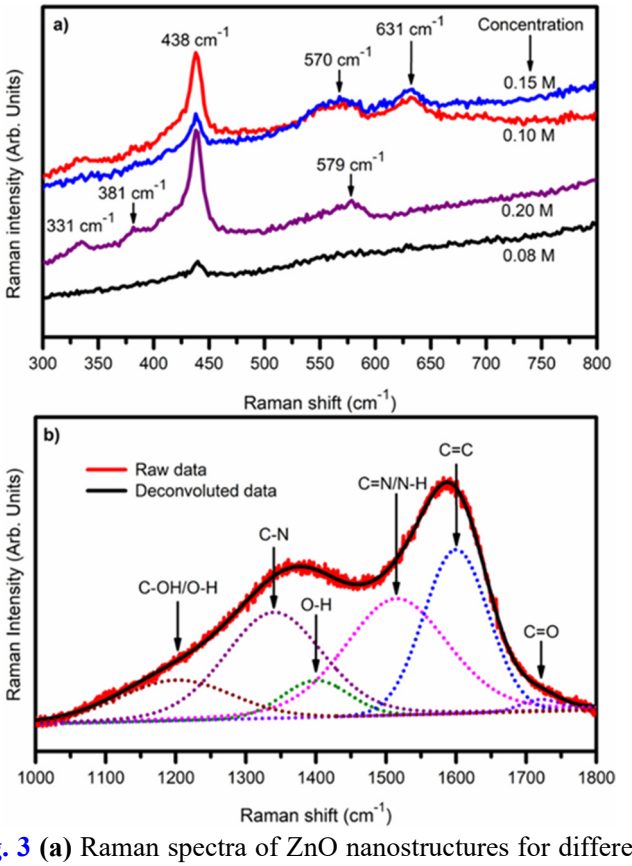

Fig. 3 **(a)** Raman spectra of ZnO nanostructures for different molar concentrations of zinc nitrate and **(b)** Raman spectra of melanin prepared using electrodeposition method.

3.4 UV-Visible spectroscopy analysis

Optical properties such as optical absorption spectra and optical band gap of ZnO and ZnO/Melanin thin films were investigated by UV-Visible spectroscopy. Fig. 4(a) and (b) shows optical absorption spectra of as-prepared ZnO and ZnO/Melanin thin films synthesized at different molar concentrations of zinc nitrate respectively. As seen in Fig. 4(a), bare ZnO films prepared at different molar concentrations of zinc nitrate absorbs mainly in the UV region whereas ZnO/Melanin films prepared at different molar concentrations of zinc nitrate absorbs significantly in the visible region [Fig. 4(b)]. This clearly indicates that melanin incorporation with ZnO increases absorption along with a slight shift in the absorption edge to the higher wavelengths.

In the direct transition semiconductor, the optical energy bandgap (E_{opt}) and the optical absorption coefficient (α) are related by,[51]

$$(\alpha E)^{1/2}=B^{1/2}(E\text{-}E_{opt}) \quad (3)$$

where α is the absorption coefficient, B is the optical density of state and E is the photon energy. The absorption coefficient (α) can be calculated from the transmittance of the films with the formula,

$$\alpha = \frac{1}{d}\ln\left(\frac{1}{T}\right) \quad (4)$$

where d is the thickness of the films and T is the transmittance. Therefore, the optical band gap is obtained by extrapolating the tangential line to the photon energy ($E = h\upsilon$) axis in the plot of $(\alpha h\upsilon)^2$ as a function of $h\upsilon$ (Tauc plot).

Fig. 4(c) and (d) shows Tauc's plot for as prepared ZnO and ZnO/Melanin thin films synthesized at different molar concentrations of zinc nitrate respectively. As seen, the bandgap energy decreases from 3.46 eV to 3.14 eV when the molar concentration of zinc nitrate precursor increases from 0.08 M to 0.2 M [Fig. 4(c)]. For ZnO/Melanin thin films, when molar concentration of zinc nitrate precursor increases from 0.08 M to 0.2 M the bandgap energy also decreases from 3.20 eV to 3.05 eV [Fig. 4(d)]. When different ZnO nanostructures are sensitized with Melanin, it helps in the injection of electrons. The decrease in bandgap energy values may be attributed to an increase in the electron mobility upon melanin incorporation in the ZnO nanostructure.

3.5 Mott-Schottky analysis

For PEC splitting of water to critically determine the usefulness of semiconductors, flat-band potential (V_{fb}) and charge carrier density (N_d) are important parameters. One of the simplest and reliable methods, reported in the literature for their estimation is through Mott-Schottky analysis. The flat band potential and charge carrier density are estimated using *Mott Schottky* equations, [52,53]

$$\frac{1}{C^2}=\frac{2}{q\,\varepsilon_0\,\varepsilon_s\,N_D}\left[V\text{-}V_{fb}\text{-}\frac{(k_BT)}{q}\right] \quad (5)$$

$$S=\frac{2}{q\,\varepsilon_0\,\varepsilon_s\,N_D} \quad (6)$$

$$w=\left[\frac{2\varepsilon_s\varepsilon_o}{qN_D}\,(V-V_{fb})\right]^{1/2} \quad (7)$$

where q is the electronic charge, ε_o is the permittivity of free space, ε_s is the dielectric constant of semiconductor electrode, k_B is Boltzman's constant, T is the temperature (in Kelvin), S is the slope of MS curve, and w is depletion layer width. With electrons as majority charge carriers, all the synthesized photo-anodes exhibited positive slopes as expected from an n-type semiconductor.[53] The slope $S = 2/q\varepsilon\varepsilon_0 N_D$ and intercept at c = 0, obtained from the plot of $1/C^2$ vs E can be used to calculate donor density and flat band potential. Fig. 5 shows the $1/C^2$ vs E plots (*Mott Schottky* plots) for all the synthesized photo-anodes. The flat band is found to shift from -0.98 V to -0.16 V vs. RHE when zinc nitrate concentration increased from 0.08 M to 0.20 M. The shift towards a negative flat band potential indicates a shift in the Fermi level towards conduction band. The shift of Fermi level towards the conduction band leads to an efficient charge transfer process across the electrolyte. The carrier density is found to increase from 7.81×10^{19} cm^{-3} and 14.03×10^{19} cm^{-3} when zinc nitrate molar concentration increased from 0.08 M to 0.20 M. The increased charge donor density is mainly responsible for improved PEC performance (discussed later) as it increases electrical conductivity. The higher electrical conductivity prolongs the lifetime of charge carriers and restrains the electron/hole recombination process.

3.6 Electrochemical impedance spectroscopy (EIS) analysis

To understand the photoelectrochemical performance of the synthesized photoanodes we have performed electrochemical impedance spectroscopy (EIS) analysis in a frequency range of 0.1 Hz to 100 kHz at a bias of 0.5 V vs RHE under UV-Visible light irradiation. Nyquist diagram of EIS data is an effectual way to measure the electron transfer resistance. The arc radius in the Nyquist plot is directly related to electron transfer resistance reflecting the energy barrier of the electrode reaction.[54] Fig. 6 shows electrochemical impedance spectroscopy (EIS) plots of all the synthesized ZnO photoanodes deposited at different concentrations of zinc nitrate. As seen the smallest arc has been observed for the ZnO photo-anode deposited for the concentration of 0.20 M i.e. for ZnO nano-sheet structure and can be assigned to the effective charge separation and minimum recombination of photo-generated charge carriers.

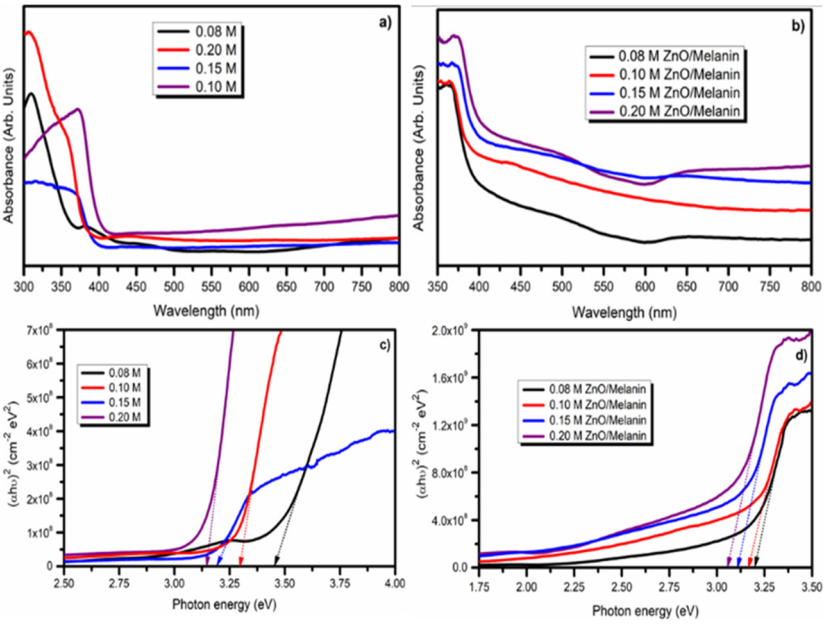

Fig. 4 UV-Visible spectra of **(a)** ZnO nanostructures synthesized at different concentrations, **(b)** melanin sensitized ZnO for different concentrations and **(c)** and **(d)** Tauc's plots for (a) and (b) respectively.

3.7 Photoelectrochemical properties

To evaluate the effect of molar concentration and melanin dye effect on PEC properties of ZnO films, the current-voltage (I-V) curves were recorded under darkness and illumination conditions. Fig. 7 show the PEC curves recorded for as-synthesized ZnO nanostructures and Melanin sensitized ZnO nanostructures at different molar concentrations of zinc nitrate. As seen in Fig. 7(a), the I-V curves of all the synthesized ZnO films demonstrated a typical feature of n-type semiconductor electrodes. Under the dark condition, the current approached to zero indicates that it is produced due to illumination of semiconductor film only and the transition time is also very small to be recorded. Significant photocurrents were recorded, especially with the film at the molar concentration of 0.2 M, suggesting well-aligned band edges with respect to redox levels corresponding to hydrogen and oxygen evolution.

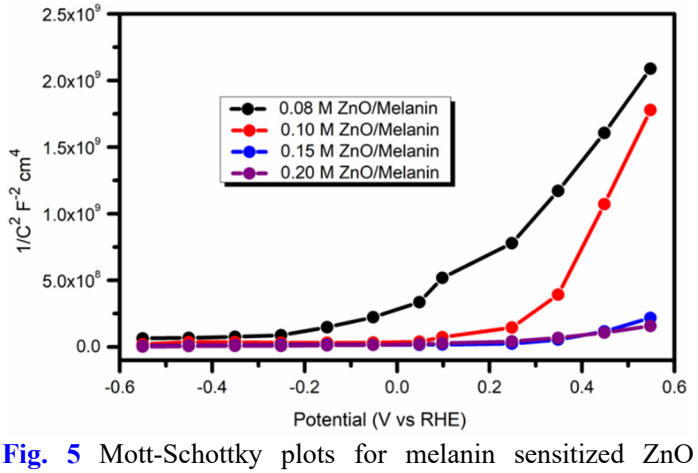

Fig. 5 Mott-Schottky plots for melanin sensitized ZnO nanostructures (at different molar concentrations of zinc nitrate).

The maximum photocurrent density was recorded for ZnO nanosheets films is around 0.2 mA/cm^{-2} at 1.4 V/RHE. Nanosheets with the concentration of 0.2 M provides high surface area and superior carrier transport, leading to the increased interfacial reaction sites and reduced recombination rate between the electrons and holes. As a result, the PEC performance of the ZnO nanosheets thin films is greatly enhanced. As depicted from melanin dye/ZnO nanosheets absorption curves, the optical absorption is also increased after melanin incorporation, and therefore all the synthesized ZnO thin films efficiently absorb visible light. The performance of melanin incorporated ZnO nanosheet (0.2 M) is remarkably better as it corresponded to J_{sc} of 0.42 mA/cm^2, as shown in Fig. 7(b). All the synthesized thin films are stable for long time illumination showing almost no loss in photocurrent even after continuous illumination for several hours. A comparison of PEC properties of various ZnO composites with the present results is shown in Table 1.

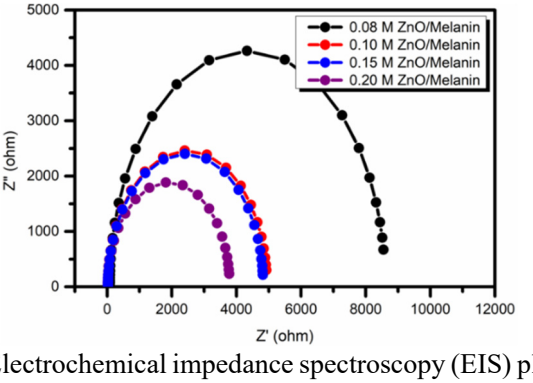

Fig. 6 Electrochemical impedance spectroscopy (EIS) plots of Melanin sensitized ZnO nanostructures (at different molar concentrations of zinc nitrate).

Table 1. A comparison of photoelectrochemical properties of various ZnO composites.

Composite Material, Morphology	Preparation method	Photocurrent density	Ref.
Chlorophyll-a/ZnO, Nanorods	Electrodeposition	0.67 mA/cm^2	[55]
Cu/ZnO, Nanocrystalline	Sol-Gel	752 μA/cm^2	[56]
CdS/ZnO, Nanorods	Spin coating	294 μA/cm^2	[57]
Co_3O_4/ZnO, Nanocrystalline	Electrodeposition	11.0 μA/cm^2	[58]
Melanin/ZnO, Nanosheets	Chemical bath deposition	0.42 mA/cm^2	Present

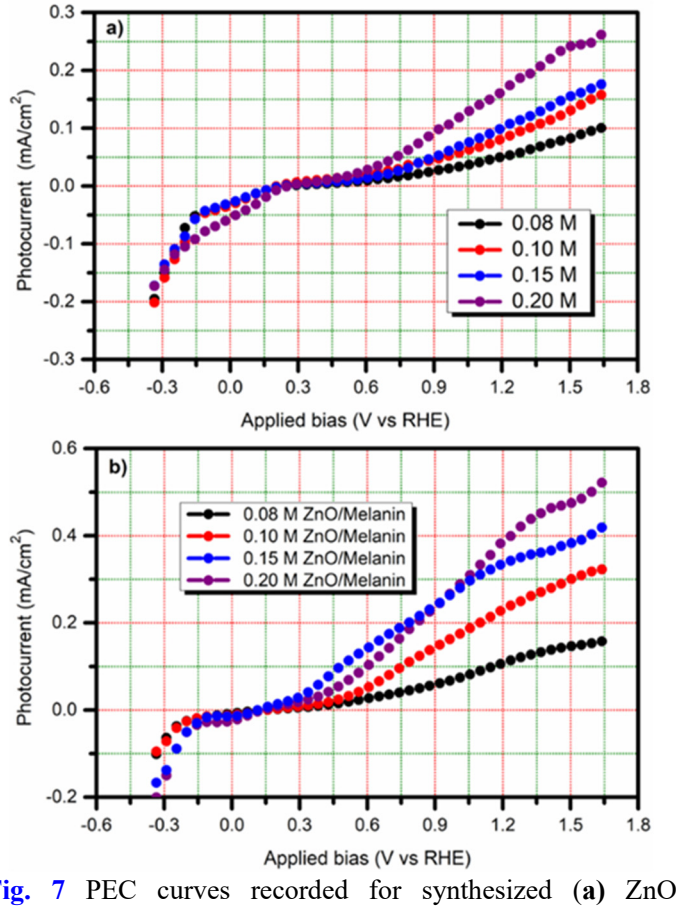

Fig. 7 PEC curves recorded for synthesized **(a)** ZnO nanostructures **(b)** Melanin sensitized ZnO nanostructures.

As seen, the maximum current density of ~ 0.42 mA/cm^2 has been observed for melanin sensitized ZnO nanosheets and it is comparable with the previously reported current density values of ZnO composites. The present work is the first attempt where PEC activity of melanin sensitized ZnO nanostructures have been undertaken. We believe that applying compositional engineering and optimizing the photoanode structure, PEC activity of melanin sensitized ZnO photoanode can be improved further. Thus, melanin incorporated ZnO can be considered as a potential material for photo-anodes for photo -splitting of water.

4. Conclusions

We have synthesized different ZnO thin films of different morphologies by chemical bath deposition and used them as photo-anodes in PEC water splitting. The working electrodes were characterized by XRD, SEM, and other optical measurements. Melanin incorporation in ZnO nanostructures extended the absorbance spectra into the visible region, thus their use in PEC splitting of water in visible light was possible. Melanin incorporated ZnO photo-anodes had shown a photocurrent density of ~0.42 mA/cm^2, which was about ~2 times that of the bare ZnO photo-anode under one sun illumination. Thus, melanin incorporated ZnO thin film can be considered as potential materials for photoanodes to generate hydrogen via the photosplitting of water.

Acknowledgement

Bharat Bade, Pratibha Shinde, Ashwini Punde, Vidya Doiphode, Shruthi Nair, Ashish Waghmare and Subhash Pandharkar are grateful to the Ministry of New and Renewable Energy (MNRE), New Delhi, for the National Renewable Energy (NRE) fellowship and financial assistance. Vidhika Sharma and Sandesh Jadkar are thankful to University Grants Commission (UPE program), New Delhi and Indo-French Centre for the Promotion of Advanced Research-CEFIPRA, Department of Science and Technology, New Delhi for special financial support.

Conflict of Interest

There is no conflict of interest.

Supporting Information

Not applicable.

References

[1] A. Fujishima and K. Honda, *Nature*, 1972, **238**, 37-38, doi: 10.1038/238037a0.

[2] M. Ni, M. Leung, D. Leung and K. Sumathy, *Renew. Sust. Energ. Rev.*, 2007, **11**, 401-425, doi: 10.1016/j.rser.2005.01.009.

[3] K. Sivula, F. Formal and M. Grätzel, *ChemSusChem*, 2011, **4**, 432-449, doi: 10.1002/cssc.201000416.

[4] S. Mali, G. Park, H. Kim, H. Kim, J. Patil and C. Hong, *Nanoscale Adv.*, 2019, **1**, 799-806, doi: 10.1039/c8na00209f.

[5] P. Dias, T. Lopes, L. Meda, L. Andrade and A. Mendes, *Phys. Chem. Chem. Phys.*, 2016, **18**, 5232-5243, doi: 10.1039/c5cp06851g.

[6] Z. Li and Z. Zhang, *Nano Res.*, 2018, **11**, 1530-1540, doi: 10.1007/s12274-017-1769-y.

[7] S. Mali, H. Kim, P. Patil and C. Hong, *Dalton T.*, 2013, **42**, 16961-16967, doi: 10.1039/c3dt51287h.

[8] Y. Hashimoto, G. Seniutinas, A. Balčytis, S. Juodkazisand Y. Nishijima, *Sci. Rep-UK*, 2016, **6**, 25010, doi: 10.1038/srep25010.

[9] Z. Chen, T. Jaramillo, T. Deutsch, A. Shwarsctein, A. Forman, N. Gaillard, R. Garland, K. Takanabe, C. Heske, M.

Sunkara and E. McFarland, *J. Mater. Res.*, 2010, **25**, 3-16, doi: 10.1557/jmr.2010.0020.
[10] J. Liu, W. Luo, K. Zhu, X. Wen, F. Xiu, J. Yuan, Z. Zou and W. Huang, *RSC Adv.*, 2017, **7**, 30650-30656, doi: 10.1039/c7ra04647b.
[11] J. Li, S. Cushing, P. Zheng, F. Meng, D. Chu and N. Wu, *Nat. Commun.*, 2013, **4**, 2651, doi: 10.1038/ncomms3651.
[12] R. Dom, L. Baby, H. Kim and P. Borse, *Int. J. Hydrogen. Energ.*, 2017, **42**, 5758-5767, doi: 10.1016/j.ijhydene.2016.12.089.
[13] U. Ozgur, Y. Alivov, C. Liu, A. Reshchikov, S. Dogan, V. Avrutin, S. Cho and H. Morkoc, *J. Appl. Phys.*, 2005, **98**, 041301, doi: 10.1063/1.1992666.
[14] S. Xiaowei and Y. Yang, *1st ed. Boca Raton*, FL CRC Press, 2016
[15] O. Kennedy, M. Coke, E. White, M. Shaffer and P. Warburton, *Mater. Lett.*, 2018, **212**, 51-53, doi: 10.016/j.matlet.2017.10.017.
[16] G. Mani and J. Rayappan, *Sensor. Actuat. B-Chem.*, 2014, **198**, 125-133, doi: 10.1016/j.snb.2014.02.101.
[17] B. Yang, A. Kumar, H. Zhang, P. Feng, R. Katiyar and Z. Wang, *J. Phys. D: Appl. Phys.*, 2009, **42(4)**, 045415, doi: 10.1088/0022-3727/42/4/045415.
[18] H. Zhang, D. Yang, S. Li, X. Ma, Y. Ji, J. Xu and D. Que, *Mater. Lett.*, 2005, **59(13)**, 1696-1700, doi: 10.1016/j.matlet.2005.01.056.
[19] B. Cao and W. Cai, *J. Phys. Chem. C*, 2008, **112(3)**, 680-685, doi: 10.1021/jp076870l.
[20] L. Xu, Q. Chen and D. Xu, *J. Phys. Chem. C*, 2007, **111(31)**, 11560-11565, doi: 10.1021/jp071536a.
[21] P. Meredith and T. Sarna, *Pigm. Cell Res.*, 2006, **19**, 572-594, doi: 10.1111/j.1600-0749.2006.00345.x.
[22] M. D'Ischia, A. Napolitano, A. Pezzella, P. Meredith and T. Sarna, *Angew. Chem. Int. Edit.*, 2009, **48**, 3914-3921, doi: 10.1002/anie.200803786.
[23] M. Tran, B. Powell and P. Meredith, *Biophys. J.*, 2006, **90**, 743-752, doi: 10.1529/biophysj.105.069096.
[24] A. Mostert, M. Sheliakina and P. Meredith, *Mater. Horiz.*, 2018, **5**, 256-263, doi: 10.1039/C7MH00831G.
[25] Y. Kim, A. Khetan, W. Wu, S. Chun, V. Viswanathan, J. Whitacre and C. Bettinger, *Adv. Mater.*, 2016, **28**, 3173-3180, doi: 10.1002/adma.201504650.
[26] S. Cho, W. Park and D. Kim, *ACS Appl. Mater. Inter.*, 2017, **9**, 101-111, doi: 10.1021/acsami.6b11304.
[27] J. Andrew, A. Clulow, A. Mostert, M. Sheliakina, A. Nelson, N. Booth, P. Burn, I. Gentle and P. Meredith, *Soft Matter*, 2017, **13**, 3954-3965, doi: 10.1039/C6SM02420C.
[28] K. Motovilov, V. Grinenko, M. Savinov, Z. Gagkaeva, L. Kadyrov, A. Pronin, Z. Bedran, E. Zhukova, A. Mostert and B. Gorshunovae, *RSC Adv.*, 2019, **9**, 3857-3867, doi: 10.1039/c8ra09093a.
[29] J. Paulin, A. Neto and C. Graeff, *J. Phys. Chem. B*, 2019, **123**, 1248-1255, doi: 10.1021/acs.jpcb.8b09694.
[30] Y. Liu, K. Ai and L. Lu, *Chem. Rev.*, 2014, **114**, 5057-5115, doi: 10.1021/cr400407a.
[31] H. Lee, S. Dellatore, W. Miller and P. Messersmith, *Science*, 2007, **318**, 426-430, doi: 10.1126/science.1147241.
[32] J. Gallas, US Patent no. US 5,036,115, Sheet 1 of 2 US 2013/00782.05 A1.
[33] M. Sheliakina, A. B. Mostert and P. Meredith, *Mater. Horiz.*, 2018, **5**, 256-263, doi: 10.1039/c7mh00831g.
[34] M. Ambrico, F. Ambrico, A. Cardone, T. Ligonzo, S. Cicco, R. Mundo, V. Augelli and G. Farinola, *Adv.Mater.*, 2011, **23**, 3332-3336, doi: 10.1002/adma.201101358.
[35] P. Kumar, E. Mauro, S. Zhang, A. Pezzella, F. Soavi, C. Santato and F. Cicoira, *J. Mater. Chem. C*, 2016, **4**, 9516-9525, doi: 10.1039/c6tc03739a.
[36] Z. Tehrani, S. Whelan, A. Mostert, J. Paulin, M. Ali, E. Ahmadi, C. Graeff, O. Guy and D. Gethin, *2D Mater.*, 2020, **7**, 024008, doi: 10.1088/2053-1583/ab72d5.
[37] Y. Kim, W. Wu, S. Chun, F. Whitacre and C. Bettinger, *P. Natl. Acad. Sci. USA*, 2013, **110**, 20912-20917, doi: 10.1073/pnas.1314345110.
[38] T. Wu, B. Wee and J. Hong, *Adv. Mater. Interfaces*, 2015, **2**, 1500203, doi: 10.1002/admi.201500203.
[39] L. Chang, F. Chen, X. Zhang, T. Kuang, M. Li, J. Hu, J. Shi, L. Lee, H. Cheng and Y. Li, *ACS Appl. Mater. Inter.*, 2017, **9**, 16553-16560, doi: 10.1021/acsami.7b03890.
[40] C. Bettinger and J. Whitacre, *US Patent no. US20150118526A1* J F 2015.
[41] C. Lee, D. Jeon, S. Bae, H. Kim, Y. Han, Y. Lee, and J. Ryu, *ChemSusChem*, 2018, **11**, 3534-3541, doi: 10.1002/cssc.201801135.
[42] B. Cullity and S. Stock, 3rd Edition, Princeton Hall (2001)
[43] N. Madkhali, H. Alqahtani, S. Alterary, H. Albrithen, A. Laref and A. Hassib, *Arab. J. Chem.*, 2020, **13**, 4987-4993, doi: 10.1016/j.arabjc.2020.01.021.
[44] A. Ismail and M. Abdullah, *J. King Saud Univ. Sci.*, 2013, **25(3)**, 209-215, doi: 10.1016/j.jksus.2012.12.004.
[45] R. Cuscó, E. Alarcón-Lladó, J. Ibáñez, L. Artús, J. Jiménez, B. Wang and M. Callahan, *Phys. Rev. B.* 2007, **75**, 165202, doi: 10.1103/PhysRevB.75.165202.
[46] D. Marquardt, *J. Appl. Math.*, 1963, **11**, 431-441.
[47] K. Levenberg, *Appl. Math.*, 1944, **2**, 164.
[48] V. Capozzi, G. Perna, A. Gallone, P. Biagi, P. Carmone, A. Fratello, G. Guida, P. Zanna and R.Cicero, *J. Mol. Struct.*, 2005, **3**, 717-721, doi: 10.1016/j.molstruc.2004.11.074.
[49] G. Perna, A. Gallone, V. Capozzi, P. F. Biagi, A. Fratello, G. Guida, P. Zanna, E. Argenzio and R. Cicero, *Phys. Scripta*, 2005, **118**, 89-92, doi: 10.1238/Physica.Topical.118a00089.
[50] L. Martinez, D. Galvao and M. Caldas, *J. Phys. Chem. B*, 1999, **103(15)**, 2993-3000, doi: 10.1021/jp983336s.
[51] J. Tauc, *Mater. Res. Bull.*, 1970, **5**, 721-729, doi: 10.1016/0025-5408(70)90112-1.
[52] I. Sero, F. Santiago, B. Denier, J. Bisquert, R. Zaera, J. Elias and C. Clement, *Appl. Phys. Lett.*, 2006, **89**, 203117, doi: 10.1063/1.2390667.
[53] F. Francisco, G. Belmonte, J. Bisquert, P. Bogdanoff and A. Zaban, *J. Electrochem. Soc.*, 2003, **150**, E293-E298, doi: 10.1149/1.1568741.

[54] J. Lin, C. Lee and K. Ho, *J. Mater. Chem.*, 2012, **22**, 1270-1273, doi: 10.1039/c1jm15227k.
[55] M. Prasad, V. Sharma, A. Mayabadi, A. Rokade, A. Pawbake, S. Rondiya, R. Waykar, A. Jadhavar, H. Pathan and S. Jadkar, *ChemistrySelect*, 2017, **2**, 1911-1916, doi: 10.1002/slct.201601814.
[56] V. Sharma, P. Kumar, J. Shrivastava, A. Solanki, V. Satsangi, S. Dass and R. Shrivastav, *J. Mater. Sci.*, 2011, **46**, 3792-3801, doi: 10.1007/s10853-011-5293-2.
[57] Y. Li, X. Zhang, S. Jiang, H. Dai, X. Sun and Y. Li, *Sol. Energ. Mat. Sol. C.*, 2015, **132**, 40-46, doi: 10.1016/j.solmat.2014.08.015.
[58] Y. Yang, W. Cheng and Y. Frank, *Appl. Surf. Sci.*, 2019, **476**, 815-821, doi: 10.1016/j.apsusc.2019.01.157.

Publisher's Note

Engineered Science Publisher remains neutral with regard to jurisdictional claims in published maps and institutional affiliations.